SLAC-PUB-11570
November 2005

A Resonant Cavity Approach to Non-Invasive, Pulse-to-Pulse Emittance Measurement*

J.S. Kim
FAR-TECH, Inc., 10350 Science Center Drive, San Diego, CA, 92121
C.D. Nantista
Stanford Linear Accelerator Center, Menlo Park, CA 94025
R.H. Miller
Stanford Linear Accelerator Center, Menlo Park, CA 94025
A.W. Weidemann
FAR-TECH, Inc., 10350 Science Center Drive, San Diego, CA, 92121/
Stanford Linear Accelerator Center, Menlo Park, CA 94025

Abstract

We present a resonant cavity approach for non-invasive, pulse-to-pulse, beam emittance measurements of non-circular multi-bunch beams. In a resonant cavity, desired field components can be enhanced up to $Q_{L\lambda}/\pi$, where $Q_{L\lambda}$ is the loaded quality factor of the resonant mode λ, when the cavity resonant mode matches the bunch frequency of a bunch-train beam pulse. In particular, a quad-cavity, with its quadrupole mode (TM_{220} for rectangular cavities) at beam operating frequency, rotated 45° with respect to the beamline, extracts the beam quadrupole moment exclusively, utilizing the symmetry of the cavity and some simple networks to suppress common modes. Six successive beam quadrupole moment measurements, performed at different betatron phases in a linear transport system determine the beam emittance, i.e. the beam size and shape in the beam's phase space, if the beam current and position at these points are known. In the presence of *x-y* beam coupling, ten measurements are required. One measurement alone provides the rms-beam size of a large aspect ratio beam. The resolution for such a measurement of rms-beam size with the rectangular quad-cavity monitor presented in this article is estimated to be on the order of ten microns. A prototype quad-cavity was fabricated and preliminary beam tests were performed at the Next Linear Collider Test Accelerator (NLCTA) at the Stanford Linear Accelerator Center (SLAC). Results were mainly limited by beam jitter and uncertainty in the beam position measurement at the cavity location. This motivated the development of a position-emittance integrated monitor.

Submitted to Review of Scientific Instruments

* Work supported by Department of Energy contracts DE-AC02-76SF00515 and DE-FG03-98ER82574.

A Resonant Cavity Approach to Non-Invasive, Pulse-to-Pulse Emittance Measurement

J.S. Kim[a)](1), C.D. Nantista (2), R.H. Miller (2), and A.W. Weidemann (1,2)

(1) FAR-TECH, Inc., 10350 Science Center Drive, San Diego, CA, 92121

(2) Stanford Linear Accelerator Center, Menlo Park, CA 94025

(Received)

ABSTRACT

We present a resonant cavity approach for non-invasive, pulse-to-pulse, beam emittance measurements of non-circular multi-bunch beams. In a resonant cavity, desired field components can be enhanced up to $Q_{L\lambda}/\pi$, where $Q_{L\lambda}$ is the loaded quality factor of the resonant mode λ, when the cavity resonant mode matches the bunch frequency of a bunch-train beam pulse. In particular, a quad-cavity, with its quadrupole mode (TM_{220} for rectangular cavities) at beam operating frequency, rotated 45° with respect to the beamline, extracts the beam quadrupole moment exclusively, utilizing the symmetry of the cavity and some simple

[a)] Electronic mail: kim@far-tech.com

networks to suppress common modes. Six successive beam quadrupole moment measurements, performed at different betatron phases in a linear transport system determine the beam emittance, i.e. the beam size and shape in the beam's phase space, if the beam current and position at these points are known. In the presence of *x-y* beam coupling, ten measurements are required. One measurement alone provides the rms-beam size of a large aspect ratio beam. The resolution for such a measurement of rms-beam size with the rectangular quad-cavity monitor presented in this article is estimated to be on the order of ten microns. A prototype quad-cavity was fabricated and preliminary beam tests were performed at the Next Linear Collider Test Accelerator (NLCTA) at the Stanford Linear Accelerator Center (SLAC). Results were mainly limited by beam jitter and uncertainty in the beam position measurement at the cavity location. This motivated the development of a position-emittance integrated monitor.[1]

I. INTRODUCTION

Beam emittance is a key beam parameter, along with beam position, for accelerator operations. This article considers a beam emittance measurement method in an X-band linear collider where beam power gets extremely high (~13 MW average and half a terawatt peak) and beam cross sections are in the sub-millimeter range. Standard emittance measurement devices such as pepper-pot foils or wire scanners are not applicable to such beams and would be vaporized by them. Currently, a non-destructive, single-pulse measurement scheme is not available for such beams, and consequently beam tune-up takes hours. A pulse-to-pulse beam emittance measurement based on striplines was first suggested by Miller, *et al.*[2] Since then several new schemes of measuring beam emittance have been presented.[3] In addition to durability, the resonant cavity approach provides stronger coupling between the beam and desired cavity mode than non-resonant approaches and a high signal-to-noise ratio by resonance of a cavity mode at the bunch frequency. The general concept of resonant cavity approach presented by Whittum and Kolomensky[4] as a beam position monitor (BPM) has been extended to measure the beam's second moment. Our initial design and measurements were reported earlier.[5,6]

In principle, it is straight-forward to extract information about the beam distribution from the cavity fields induced by the beam. For instance, the zeroth order beam moment, proportional to the total charge, can be obtained from the monopole mode, the first order beam moments from the *x*- and *y*-dipole modes and utilizing the zeroth order beam moment, then the second beam moments from the quadrupole modes and the zeroth and the first order beam moments and so on. In practice, due to the so-called common-mode-problem, it is not easy to isolate the information of each of the beam moment independently. The common-mode problems can be minimized by hybrid networks that subtract the fields of unwanted modes using symmetry. There is another limiting effect on beam moment measurement resolution. It is the signal to noise ratio. Signal to noise can be enhanced by utilizing a resonance cavity with multi-bunches. In some rf linac designs, each beam pulse consists of many bunches arriving at a well-defined rate. As a train of bunches goes through a cavity, the field of the mode is enhanced by resonance up to Q_L/π , the loaded quality factor divided by π, while the other cavity modes are off resonance.

In this manuscript, a resonant cavity approach is presented for beam second moment measurement by employing a resonant cavity monitor operated at its quadrupole mode (TM_{220} for a rectangular cavity). A resonant cavity (quad-cavity) can be designed, by symmetry, to have a mode that is exclusively excited by the beam's quadrupole moment. The hybrid networks are a crucial component of this approach, and serve to minimize the parasitic common mode effects. The common mode effects can be further minimized by: (1) separating the other resonant mode frequencies away from the operating resonant mode; (2) maximizing the beam and the operating mode coupling by optimizing the cavity length along the beam pipe; and (3) utilizing symmetry in simple networks to cancel out parasitic modes. The monopole and dipole modes could be completely isolated via proper hybrid T connections, if perfect symmetry can be achieved.

To demonstrate the resonant cavity approach for a beam monitor, a square or near-square rectangular cavity is chosen. In such a cavity, the lowest monopole mode and the "accelerating mode" is TM_{110}, the lowest dipole modes or first two "position-sensitive" modes are TM_{210} and TM_{120}, and the lowest quadrupole mode is TM_{220}. The next higher modes are TM_{310} and TM_{130}. It is interesting to note that, for a square cavity, the sum of the degenerate TM_{130} and TM_{310}

modes yields a monopole-like field pattern and the difference of the modes yields a field pattern which has the nature of the normal quadrupole mode near the axis.

More generally, the rectangular cavity modes TM_{λ}, with $\lambda \equiv n_x, n_y, n_z$ and n_z=0,fall into three classes with respect to their field pattern symmetries. The symmetry planes of $x = 0$ and $y = 0$ are shown in Fig. 1, along with the cavity cross section dimensions, L_x and L_y. The symmetry of the electric fields of the modes,

$$E_{z,\lambda} = \sin\beta_x\left(x - \frac{L_x}{2}\right)\sin\beta_y\left(y - \frac{L_y}{2}\right), \text{ where } \beta_x = n_x\pi / L_x \text{ and } \beta_y = n_y\pi / L_y, \tag{1}$$

depends on the odd or even nature of the mode numbers n_x and n_y:

$$\begin{array}{ll} n_x = odd \;\; and \;\; n_y = odd; & monopole\text{-}like \\ n_x = odd \; and \;\; n_y = even, \;\; or \;\; n_x = even \; and \;\; n_y = odd; & dipole\text{-}like \\ n_x = even \;\; and \; n_y = even; & quadrupole\text{-}like \end{array} \tag{2}$$

where the mode labels such as 'monopole-like' are given according to the leading field harmonic of the mode. Note that an odd index gives an even symmetry across the center and an even index gives an odd symmetry. The mode symmetry is preserved even with a circular beampipe attached, since the beam pipe does not break these symmetries. This symmetry property, along with proper networks, leads to a design of a cavity that is sensitive exclusively to the beam quadrupole moment.

The hybrid tees, as depicted in Fig. 2, in principle, can completely eliminate the contributions from unwanted modes, all with even-even, odd-even, and even-odd symmetry of E_z. Then, having odd-odd symmetry, the lowest surviving quadrupole mode is TM_{220}. The next higher contributing TM modes, TM_{420} and TM_{240}, are also quadrupole in nature, but resonate more than fifty percent higher in frequency than the TM_{220} mode.

In order to maximize the measurement resolution of the beam quadrupole moment, maximum coupling between the beam and the lowest quadrupole cavity mode is required. Accelerator beams in focusing and defocusing (FODO) lattices generally have upright bi-Gaussian distributions in the beamline coordinates. Consequently, the simplest rectangular quadrupole pickup cavity would be square, use the $n_x = 2$ and $n_y = 2$ mode, and be rotated by 45° with respect to the beamline, resulting in a diamond configuration when looking into the beampipe as shown in Fig. 2. This TM_{220} mode would measure only the normal quadrupole beam moment (in the laboratory coordinates).

When the cavity orientation is rotated, the cavity coordinates shown in Fig. 1 and the laboratory coordinates do not coincide. Although cumbersome, for clarity, throughout this paper, we use (x_L, y_L, z) as shown in Fig. 2 for the beam, or the linac coordinates, and reserve the x, y, and z coordinates for the cavity coordinates. Explicitly, the quadrupole beam moment we are interested in is as follows.

$$< x_L{}^2 - y_L{}^2 > = < x_{L,b} >^2 - < y_{L,b} >^2 + \sigma_{x_L}^2 - \sigma_{y_L}^2 \qquad (3)$$

Here, σ_{x_L} and σ_{y_L} are rms-beam-sizes and $<x_{L,b}>$ and $<y_{L,b}>$ are beam positions, the first order beam moments, represented in the linac coordinate system. The angled brackets denote spatial the average over the charge distribution. It indicates that the quantity $\sigma_{x_L}^2 - \sigma_{y_L}^2$ can be obtained from a single quadrupole-moment measurement if the beam position is known. A series of such monitors placed in a FODO lattice, and separated by an adequate machine phase advance, permits one to deconvolve the beam Twiss parameters and rms emittance. In order to maximize the signal to noise level of the measurement, one can measure the signals near the magnets of the FODO lattice, where the beam has its largest aspect ratios. The quad-cavity system measures the beam emittance by selectively measuring the output voltage that is proportional to the beam moment $< x_L{}^2 - y_L{}^2 >$.

With this introduction, we present more details of the quad-cavity monitor design as follows. The basic emittance measurement concept is given in Sec. II, the basic concepts of cavity-beam interaction and beam rms size measurement are in Sec. III, computer simulations in Sec. IV, signal calibration in Sec. V, and fabrication considerations in Sec. VI. Then, in Sec. VII we present cold tests, tuning of a prototype cavity, and the beam tests, followed by a discussion in Sec. VIII.

II. BEAM EMITTANCE MEASUREMENT VIA QUADRUPOLE MOMENT

The beam emittance measurement with a quadrupole cavity relies on the beam optics considerations given in this section The beam emittance at a reference plane in an accelerator may be represented by an ellipsoid in the trace space, defined as $X^T(0)\,\sigma^{-1}(0)\,X(0) = I$. The argument 0 indicates a reference plane, $X = (x_L, x'_L, y_L, y'_L, \;\; ... \;\;)^T$ is a $2n$-dimensional column vector, and σ is a $2n \times 2n$ symmetric matrix containing the beam parameters. For instance, $\sigma_{11} = (\sigma_{x_L})^2_{rms}$ where $(\sigma_{x_L})_{rms}$ is the root-mean-square in the x_L-spread of the beam. Considering only the beam optics in the space transverse to the beam-pipe, ignoring longitudinal beam coupling with the transverse, the beam parameter matrix has the following form.

$$\sigma = \begin{pmatrix} \begin{pmatrix} \sigma_{11} & \sigma_{12} \\ \sigma_{12} & \sigma_{22} \end{pmatrix} & \begin{pmatrix} \sigma_{13} & \sigma_{14} \\ \sigma_{23} & \sigma_{24} \end{pmatrix} \\ \begin{pmatrix} \sigma_{13} & \sigma_{14} \\ \sigma_{23} & \sigma_{24} \end{pmatrix} & \begin{pmatrix} \sigma_{33} & \sigma_{34} \\ \sigma_{34} & \sigma_{44} \end{pmatrix} \end{pmatrix} \tag{4}$$

When the $x_L - y_L$ coupling of the beam is negligible, the off-diagonal 2×2 block sub-matrices of the σ matrix become zero. In this case, the σ matrix is completely described by six beam parameters, $\sigma_{11}, \sigma_{12}, \sigma_{22}, \sigma_{33}, \sigma_{34}$ and σ_{44}. Thus, six independent quadrupole signal measurement, $\sigma_{11} - \sigma_{33}$, can determine the beam emittance in the $x_L - y_L$ space completely.

For a matched beam, if the beam betatron function is periodic with respect to the chosen interval, one obtains

$$\frac{\sigma_{11}}{\sigma_{33}} = \frac{1+\sin(\mu/2)}{1-\sin(\mu/2)}, \quad \text{and} \quad \sigma_{11} - \sigma_{33} = \varepsilon \frac{2L}{\cos(\mu/2)}, \tag{5}$$

where $\sin(\mu/2) = L/(2f)$, μ is the betatron phase advance between the interval distance L, and f the focal length of the FODO magnets.

In order to obtain independent measurements it is better to have large values of $\sigma_{11} - \sigma_{33}$, as long as the beam is not lost. Note that the $\sigma_{11} - \sigma_{33}$ becomes infinite at $\mu = \pi$, indicating beam loss. A value of $\mu \approx 120^\circ$ can be a good choice. Six consecutive measurements of quadrupole signals at or near the quadrupole magnets will provide six independent equations for the six emittance parameters.

When there is some misalignment of the magnets, $x_L - y_L$ coupling will be present. In this case, the off-diagonal terms of the transfer matrix should be taken into account, requiring four additional measurements for full beam emittance determination. The four additional measurements may be performed by adding four additional quad-cavity measurement systems, rotated by 45° around the beampipe, near the six measurements mentioned above. One can consider replacing four of the six systems by a double quad-cavity measurement system whose cavities are rotated 45° degrees to each other. In practice, however, one should align the magnets until the $x_L - y_L$ couplings become negligible, thus requiring only six measurements.

With one measurement alone, beam rms size, the longer dimension of the cross-section, can be measured for an elongated cross-section beam. A quad cavity providing such a measurement is described below.

III. CAVITY-BEAM INTERACTION AND BEAM RMS SIZE MEASUREMENT

The basic concept of the interaction between a beam and cavity mode is well described in Whittum and Kolomensky.[4]

A. Single bunch vs. multi-bunches

The cavity voltage excited by the beams may be described as a driven, damped, simple harmonic oscillator. The drive term is proportional to the time-derivative of the interaction between the beam current I_b and the cavity fields and the damping is inversely proportional to the loaded quality factor of the mode $Q_{L\lambda}$. The derivation of the model is well described in reference [4]. As in Eq. (25) of the reference, the time-behavior of the voltage radiated from a beam-driven cavity mode is described as follows.[7]

$$\left(\frac{d^2}{dt^2}+\frac{\omega_\lambda}{Q_{L\lambda}}\frac{d}{dt}+\omega_\lambda^2\right)V_\lambda(t;r_\perp)\approx\frac{1}{2}\omega_\lambda\left[\frac{R}{Q}\right]_\lambda\frac{d}{dt}I_b(t;r_\perp)=2k_\lambda\frac{d}{dt}I_b(t;r_\perp)\,. \tag{6}$$

This loaded quality factor $Q_{L\lambda}$ describes the overall sharpness of the cavity mode's frequency response. It is related to the unloaded quality factor $Q_{w\lambda}$ and the external quality factor $Q_{e\lambda}$, which are the stored mode energy divided by the energy dissipated or emitted per rf cycle, respectively, through

$$\frac{1}{Q_{L\lambda}} = \frac{1}{Q_{w\lambda}} + \frac{1}{Q_{e\lambda}} . \tag{7}$$

The subscript λ refers to *m, d* and *q* for the monopole mode, the dipole mode, and the quadrupole mode, respectively, following their leading field harmonic. The quantity [*R/Q*], which is the shunt impedance divided by the unloaded quality factor, is a measure of beam coupling with the cavity fields. Employing the accelerator convention *R* = (energy gain per unit charge)$^2/P_{dis}$, or equivalently $R = |\tilde{V}|^2 / P_{dis}$, using the peak synchronous cavity voltage, it has the well known relationship to the cavity voltage,

$$\left[\frac{R}{Q}\right]_{r_\perp,\lambda} = \frac{\left|\tilde{V}_\lambda(r_\perp)\right|^2}{\omega_\lambda U_\lambda} \equiv \frac{4}{\omega_\lambda} k_{r_\perp,\lambda} , \tag{8}$$

where $k_{r_\perp,\lambda}$ is the loss factor, and $U_\lambda = 1/(2\varepsilon_0)$ is the normalized cavity mode energy. The factor ½ in the middle of Eq. (6) accounts for the fact that [*R/Q*] is defined using the peak voltage, while the voltage V_λ in the circuit equation is the rms value. The tilde notation is used for variables in frequency space.

Equation (6) is a differential equation which depends on only time, and is separable in the spatial and time variables. The time dependent part is essentially the same for all modes and thus it needs to be solved only once for one mode. Using Laplace's method, we obtain the time dependent solution of the equation after a beam has passed the cavity.[8,9] The spatial dependence of the voltage response near the axis can be easily obtained from the field dependence in x and y.

single Gaussian (in t) bunch

For a single bunch with the Gaussian current,

$$I_b = \frac{Q_b}{\sqrt{2\pi}\sigma_t}\exp\left(-\frac{(t-t_b)^2}{2\sigma_t^2}\right),$$

where Q_b is bunch charge, t_b is bunch arrival time. The cavity voltage response has the following solution,

$$V_\lambda(t,\vec{r}_\perp) = -2K_\lambda Q_b \exp\left[-\frac{1}{2}\omega_\lambda^2\sigma_t^2\right]\exp\left(-(t-t_b)\Gamma_\lambda\right)\cos\omega_\lambda(t-t_b)\,H(t-t_b)\,, \qquad (9)$$

where the Heaviside step function defined as

$$H(x) \equiv \begin{cases} 0 & for \quad x<0 \\ 1 & for \quad x>0 \end{cases}.$$

The response of a point current, $I_b(t) = Q_b\delta(t-t_b)$, can be obtained by simply taking the limit of infinitesimal beam length in z (or t) in Eq.(9).

multi-bunch responses

Multi-bunch responses can be obtained by summing over the single bunch responses at times delayed by the bunch interval τ. For a train of N-bunches, the amplitude of the sinusoidal voltage just after the n^{th} bunch is,

$$\left|V_\lambda^N(t_n)/V_\lambda^N(t_0)\right| = \left|(1-\exp(-\Gamma n\tau))/(1-\exp(-\Gamma\tau))\right|$$

with $t_n = t_0 + (n-1)\tau$ for $n = 1,2,\cdots,N$,

and

$$\left|V_\lambda^N(t > t_N)\right| = \left|V_\lambda^N(t_N)\exp(-\Gamma(t-t_N))\right| \quad \text{for} \quad t > t_N .$$

Fig. 3 shows the voltage amplitude for 900 bunches, filling every potential bucket, when the mode frequency is at perfect resonance with the bunch frequency $f_0 = 11.424$ GHz (upper curve), when it is mismatched by $\delta f = f_0/(2Q_{L\lambda})$ = 7.6 MHz with $Q_{L\lambda}$ = 750 (middle curve), and when it is mismatched by $2\delta f$ (bottom curve).

The asymptotic voltage for infinitely many bunches is shown in Fig. 4 for $0.9\,\omega_{RF} \le \omega_\lambda \le 3.2\,\omega_{RF}$, where ω_{RF} is the accelerator rf frequency at which the beam is bunched,

$$\underset{N->\infty}{Lim}\left|\frac{V_\lambda^N(t)}{V_\lambda^N(t_0)}\right| = \left|1-\exp\left(\frac{\pi}{Q_{L\lambda}}\frac{\omega_\lambda}{\omega_{RF}} - 2\pi i\frac{\omega_\lambda}{\omega_{RF}}\right)\right|^{-1}. \tag{10}$$

Approximating the asymptotic value around integer values as $\omega_\lambda / \omega_{RF} = h + \delta$, with h being the bunch separation in rf wavelength, we obtain that the output voltage of the resonant mode is enhanced at multiples of the fundamental resonance by the factor of $Q_{L\lambda}/(\pi h)$, a potentially large number, but decreasing with *h*. The enhancement of the desired signal, suppression of the unwanted signals, and practical fabrication issues such as tolerance determine the design specification.

B. Analytic pillbox model

A closed pillbox is a good starting point for resonance cavity design, since we know analytic solutions for all the resonance fields and frequencies.

The cavity fields of TM modes, with cavity dimensions L_x, L_y and L_z, were introduced in the Introduction. The electric fields, Eq.(1), can be expanded in terms of $\beta_x x \equiv n_x \pi x / L_x << 1$ and $\beta_y y \equiv n_y \pi y / L_y << 1$ near the origin.

$$E_{z,\lambda} = \begin{cases} 1-(\beta_x x)^2/2-(\beta_y y)^2/2+\cdots & for \quad n_x = odd, n_y = odd \\ (\beta_x x)-(\beta_x x)(\beta_y y)^2/2-(\beta_y y)^3/6+\cdots & for \quad n_x = even, n_y = odd \\ (\beta_y y)-(\beta_y y)(\beta_x x)^2/2-(\beta_x x)^3/6+\cdots & for \quad n_x = odd, n_y = even \\ (\beta_x x)(\beta_y y)+\cdots & for \quad n_x = even, n_y = even \end{cases} \tag{11}$$

Although there is a distinct difference between a closed pillbox and a cavity with a beampipe, and the cavity resonant mode fields and those of the synchronous harmonic have different expansions, we can associate each cavity mode with its dominant spatial dependence. In that, a closed pillbox calculation provides a good reference and starting point of our cavity design.

With the electric field of a pillbox given in Eq. (1) and the remaining non-vanishing components of TM modes,

$$Z_0 H_{x,\lambda} = j\frac{\beta_y}{\beta_\lambda}\sin\beta_x\left(x-L_x/2\right)\cos\beta_y\left(y-L_y/2\right), \text{ and} \tag{12}$$

$$Z_0 H_{y,\lambda} = -j\frac{\beta_x}{\beta_\lambda}\cos\beta_x\left(x-L_x/2\right)\sin\beta_y\left(y-L_y/2\right)$$

where $Z_0 = (\mu_0 / \varepsilon_0)^{-1/2} \approx 377$ Ohms, $\beta_x = n_x \pi / L_x$, $\beta_y = n\pi / L_y$, and $\beta_\lambda = \sqrt{\beta_x^2 + \beta_y^2}$. Various important quantities such as resonant frequencies, output powers, and shunt impedances can be estimated if cavity dimensions are given. In addition, the wall quality factor (Q_w) can be obtained from $Q_w^{-1} = (\delta / 2)(\int dS |\tilde{H}|^2 / \int dV |\tilde{H}|^2)$, where the skin-depth $\delta \approx 2.1 \mu m \big/ \sqrt{f(GHz)} \approx 1.2 \mu m$ for OFE copper at $f = 11.424$ GHz.

The cavity dimensions can be determined by the resonant frequency and the transit-time angle. The maximum transit factor occurs at transit angle $\theta_q = 133.56^\circ$, which leads to an axial cavity dimension of 0.9736 cm for the quadrupole mode. Together with the cross-section dimensions of the cavity whose TM_{220} mode resonates at 11.424 GHz, the cavity dimensions are determined to be:

$$L_x = L_y = 3.7112\, cm = 1.46110\, in, \quad L_z = 0.9736\, cm = 0.38330\, in. \tag{13}$$

Using the analytic electric and magnetic fields in Eqs. (1) and (12), useful quantities are evaluated for a 1 nC bunch traveling at $x = y$ in mm away from the axis. Table I shows these values: the resonant frequencies of the lowest cavity modes, their leading term in field harmonics, skin depths, the wall quality factors, kick factors (k_λ), [R/Q] values, field energy of the cavity mode ($U_\lambda = k_\lambda \times Q_b^2$), the peak power ($P_\lambda = \omega_\lambda U_\lambda / Q_{e,\lambda}$) radiated out of the cavity from each of the modes, and the expected power of each mode filtered around the operating frequency, assuming the resonance response of each cavity mode is of Lorentzian shape,

$$P(\omega) \propto |E(\omega)|^2 \propto \frac{1}{(\omega-\omega_\lambda)^2 + (\omega_\lambda / 2Q_\lambda)^2} . \tag{14}$$

Note that, when critically coupled, $Q_{e,\lambda} = Q_{w,\lambda}$. The filtered power around a frequency away from its resonant frequency can then be determined as follows.

$$P_\lambda(\textit{filtered around } \omega) = \left[(2Q_{L\lambda})^2 \left(\frac{\omega}{\omega_\lambda} - 1 \right)^2 + 1 \right]^{-1} \times P_\lambda(\omega_\lambda) \tag{15}$$

The power filtered around a frequency far away from a resonant mode frequency is much smaller than its peak power. This power reduction due to being off-resonance is 4×10^{-8} for the dipole mode and 10^{-7} for the TM_{310}+TM_{130} monopole-like mode when filtered around 11.424GHz.

The analytic estimates in Table I compare well with the HFSS[10] and the GdfdL [11] simulations.

C. Beampipe effect on the resonant frequencies

The effect of the beampipe on resonant frequencies has been investigated. For this study, the transverse dimensions of the cavity are fixed at 3.7113cm × 3.7113 cm and the radius of the beampipe is varied from 0 (closed pillbox), through 6.5 mm. Since the resonant frequencies depend only on the ratio of the beampipe size to the cavity dimensions, we present the results in terms of the ratio of the diameter to the cavity dimension, from 0 to 0.35. Fig. 5 shows the frequency variation. As the beampipe dimension is increased, the monopole frequencies increase, while the dipole and quadrupole frequencies decrease. If we consider the transition from pillbox to cavity with beampipe to proceed from a small perturbation of the cavity walls, the frequency trend can be understood from Slater's perturbation theorem[12]. This states that a perturbation of a cavity wall which increases the volume raises the resonant frequency if the perturbation is at a region of high electric field and lowers the frequency if it is at a region of predominantly magnetic field. The monopole frequencies have electric field on axis; the other modes have more magnetic field near the beampipe region. The frequency modification by the beampipe is found to be rather small for all modes, as shown in Fig. 5.

Utilizing maximum available symmetry of the geometry, only 1/8 of the geometry needs to be modeled while varying boundary conditions on the symmetry planes as follows.

$$\begin{array}{llll} x=0 \quad magnetic; & y=0 \quad magnetic; & for & monopoles \\ x=0 \quad electric; & y=0 \quad magnetic; & for & y-dipoles \\ x=0 \quad magnetic; & y=0 \quad electric; & for & x-dipoles \\ x=0 \quad electric; & y=0 \quad electric; & for & quadrupoles \end{array}$$

z = 0 electric for all cases

There are few things to note. In a square cavity, the TM_{210} and TM_{120} modes are degenerate. Therefore, any combination of TM_{210} and TM_{120} is also a solution. To be seen later, the quad-cavity is not perfectly square when the hybrid network waveguides are attached, and thus the dipole modes are no longer degenerate. The dipole modes are then the x- and y-dipole modes. The TM_{310} and TM_{130} are also degenerate in a square pillbox. The degeneracy is removed with a beampipe attached at the center. The two modes are $TM_{310} \pm TM_{130}$. The sum mode is a predominantly monopole, and the difference mode corresponds to the 'normal' quadrupole mode with its electric field being proportional to $x^2 - y^2$. As expected, the resonant frequency is increased with beampipe radius for the predominantly monopole modes (TM_{110}, and the sum of TM_{310} and TM_{130}), while the opposite occurres for the predominantly dipole modes (TM_{210} and TM_{120}) and the quadrupole modes (TM_{220}, and TM_{310}-TM_{130}).

D. RMS beam-size measurement resolution based on a pillbox model

The quality of the quad-cavity monitor ultimately depends on the measurement resolution of the quadrupole moment. A reasonable estimate can be made using a 3-D electromagnetic field solver without the beams. HFSS simulations were performed for a cavity with a beampipe attached to evaluate the similar quantities in Table I for the *x*-dipole, the quadrupole, and the monopole-like TM_{310}+TM_{130} mode. The results are presented in Table II. Presented are the resonant frequencies, Q_w, the synchronous integral and power dissipated through the walls, for chosen beam offsets (r_b), using the normalized fields by the code. The values of shunt impedance R and output power P_{out} are then evaluated for the Next Linear Collider (NLC) beams of 1 nC per bunch operating at 714 MHz (bunch current = 0.714 A) as follows.

$$R = \frac{|\tilde{V}|^2}{P_{dis}}$$

$$P_{out} = \frac{\beta}{(1+\beta)^2} I_b^2 R \quad \text{where} \quad I_b = Q_b f_b . \qquad (16)$$

Here $\beta \equiv Q_e / Q_w = P_{out} / P_{dis}$, and Q_b and f_b are bunch charge and bunch frequency. Note that the shunt impedance is independent of normalization used in the simulation. The synchronous voltage integral and power dissipated to walls (P_{dis}) are obtained from HFSS.

In order to be resolved, the quadrupole signal must be greater than other parasitic signals filtered around the quadrupole frequency. The critical lengths that satisfy the condition are 28 μm with respect to the TM_{110} signal, 0.4 μm with respect to the TM_{120} or TM_{210} signals, and 120 μm with respect to the TM_{310}+TM_{130} signal. Consequently, the quadrupole resolution is limited to $x = y = 120$ μm without any hybrid tee networks or the resonance enhancement by multi-bunches. To enhance the rms-beam-size measurement resolution from 120 $\times\sqrt{2}$ μm to 1 μm, a reduction of $\sim 10^{-9}$ of the common mode power is required. One can eliminate the common mode effect completely via hybrid tee networks if the network and the cavity symmetry are perfect, though in practice a small error may exist. The resolution analysis presented here was obtained with a off-centered pencil beam in one cavity quadrant. For the x_L^2-dependent quadrupole field, this is equivalent to a flat, centered, Gaussian distribution with rms beam size equal to the diagonal off-axis distance of the pencil beam.

Another limit is detectability. In order to estimate the measurable rms-beam-size resolution, the measurable power ($P_{measurable}$) above electronic noise is assumed to be 10^{-11} W, about 250 times the thermal noise. The thermal noise of electronic measurements with bandwidth of 10 MHz at room temperature is 4×10^{-14} W, which can be derived from the following formula: $P_{thermal}(W) = k(Joule/Kelvin)\,T(Kelvin)\,B(bandwidth\ in\ Hz)$. With this measurable power, from

$$\begin{aligned} resolution\ of\ rms-beam-size &= r_b\left(\frac{P_{q,out}}{P_{measurable}}\right)^{1/4} \\ resolution\ of\ beam\ position &= r_b\left(\frac{P_{d,out}}{P_{measurable}}\right)^{1/2} \end{aligned} \quad , \tag{17}$$

the quadrupole resolution is 6 μm for a single bunch. For multi-bunches in a single shot, due to resonance enhancement, the quadrupole output power can be enhanced by $(Q_L/\pi)^2$. Thus, an rms-beam-size as small as 0.2 μm might be measurable. Together with the common mode constraints, we conclude that the quadrupole resolution should be on the order of a micronmeter.

IV. COMPUTER SIMULATION

Based on the resonant cavity concept described in the previous sections, a specific design of a quad-cavity is presented here as an application for X-band accelerators operating at 11.424 GHz. The diameter of the beam pipe attached to the quad-cavity was chosen to be 1 cm, large enough for an X-band linac. Note that the cut-off of the TE_{11} mode of this cylindrical beam-pipe corresponds to 17.6 GHz. The choice of loaded Q was determined by considering the following competing conditions: both the resonant enhancement and the tolerance requirement increase with increasing Q_{Lq}. A Q_{Lq} value around 1000 is chosen, for which the FWHM of the resonant mode is 10 MHz.

With these conditions, after detailed numerical simulations using the electromagnetic field-solver HFSS [10], an optimized quad-cavity design is obtained and is shown in Fig. 6. The hybrid network waveguides are attached to only two sides of the cavity. The x- and y-dimensions of the cavity were adjusted slightly so as to compensate for the field leakage through the irises. The design parameters are as follows.

Beam pipe diameter = 1 cm
Cavity axial dimension (L_z) = 0.97 cm
Cavity transverse dimensions = 1.457'' by 1.417'' (18)
Waveguide WR62 inner dimensions= 0.622'' by 0.311''

In order to study the time behavior of the beam and cavity interaction, the main components of the quad-cavity system were modeled with the GdfidL code.[11] This model is the same as the 3-D figure in Fig. 6, except for the last hybrid network and the 90° bend waveguides. It includes the main cavity, the beampipe, and the two hybrid tees until just before they start bending. The model has two waveguide ports as indicated in the figure in addition to the beampipe ports. Numerical simulations were performed for a single bunch, modeled as a pencil beam with a Gaussian shape in t, $\sigma_z = c\sigma_t = 4\ mm$, for numerical resolution and with an offset $x = y = 0.5\ mm$ in the cavity coordinates. The large bunch length reduces the magnitude of the output voltage via the exponential factor in Eq. (9). This factor is 0.67 for the operating resonant frequency, since $\omega_q \sigma_t \approx 0.92$. Thus the simulation voltage needs to be multiplied by 1.5 for much shorter bunches and the output power by 2.25.

An off-centered bunch at $x = y = 0.5\ mm$ generates the monopole, the dipole and quadrupole modes in the cavity. The three hybrid tee waveguide-networks in the design subtract the fields through the irises. The simulation model includes the first two hybrid T's attached to the cavity, which provides a subtraction of the electric fields through the two irises on the cavity, eliminating the components from the monopoles and one of the dipoles. The results of the simulation are presented in Fig. 7. The first plot shows output voltage (V1) from one of the ports, port 1, which includes the quadrupole and one of the x- or y- dipole modes. Similarly, the other port voltage (V2) includes the quadrupole and the same dipole mode as in V1. By taking the difference of V1 and V2, we accomplish the effect of the last hybrid network that provides a subtraction of the fields, although this is not modeled. This difference signal V1-V2 is shown in the second plot of the figure. The external Q of the quadrupole mode can be obtained from the slope of the envelope of V1-V2, when plotted on a logarithmic scale. It is roughly 1000. The sum voltage (V1+V2), which is proportional to the dipole mode, survives after the first pair of networks, has a similar behavior as the first plot, and is not shown. If we had another pencil beam at $x = y = -0.5\ mm$ to cancel the dipole moment, the sum voltage will indeed be zero except numerical noise. The second beam would just interchange V1 with -V2 and V2 with -V1. The sum signal of the two pencil beams would be $(\mathrm{V1-V2}) + (\mathrm{V2-V1}) = 0$, reflecting the true absence of a dipole moment for a symmetric centered beam.

The third plot in Fig. 7 shows the difference signal V1-V2 for 80 ns long pulse with about 900 bunches filled in every potential bucket. The response of a pulse that contains a train of bunches can be obtained by superposing the port signals of a single bunch at delayed times, each delayed by the bunch intervals $1/f_0$, where f0=11.424 GHz. The amplitude of the quad signal (V1-V2) increases monotonically with the number of bunches indicating a good resonance. If the bunch frequency is slightly mismatched with the cavity resonant frequency the quad-signals exhibit some modulation, as an extension of Fig. 7 would predict, and saturate at a reduced amplitude. This result is not presented. The amplitude of the multi-bunch difference signal shown in the third plot is about 180 times larger than that of a single-bunch. The value is somewhat smaller than the ideal maximum $Q_{Lq}/\pi \approx 240$. This slight discrepancy may be due to finite length of bunch used in our numerical modeling, numerical inaccuracies, and slight resonant frequency error of the cavity. The last plot shows the multi-bunch sum signal, (V1+V2), which is clearly non-resonating with the multi-bunches.

Simulations at different beam locations (at $x = y = 0.5\ mm$, $x = y = 1\ mm$, and $x = y = 1.5\ mm$) verified that the difference-voltage increased quadratically with offset, while the sum-signal increased linearly with offset.

The power spectra of the output voltages provide useful information. (See Fig. 8.) We show only the lowest waveguide mode results, since the next higher modes have frequencies above 16 GHz, and thus their contribution to the spectrum around 11.424 GHz is negligible. The output voltage V1 (top plot) of a port shows several significant frequencies. The other port has similar behavior, cannot be distinguished in the scale presented, and thus is not shown. The sum voltage V1+V2 (second plot) of the two ports has a peak at the dipole frequency, while the difference voltage V1-V2 (third plot) shows a peak at the quadrupole, 11.424 GHz, frequency.

With multi-bunches, the sum voltage (fourth plot) and the difference voltage (fifth plot) show a peak at 11.424 GHz. The fourth plot is the multi-bunch resonant enhancement of the non-zero component around 11.424 GHz of the dipole mode resonating at 8.848 GHz. Its enhancement factor is exactly the same as that of the quadrupole. Therefore, resonant enhancement does not increase the common mode resolution. Rather, the resonance enhancement increases resolution with respect to the detectable power over noise.

The area under each spectrum near the operating frequency is proportional to the output voltage around that frequency. (The vertical axis of all the spectrum plots is in units of $\sqrt{Power(Watt)}\,/\,Hz$, up to a constant.) The quadrupole resolution can be estimated from the last two cases in the figure. When we magnify the spectrum near the quadrupole frequency the shapes of the spectra are similar to each other. From this information for a bunch at $x = y = 0.5\ mm$, we can estimate the location of a bunch where the output power from the quadrupole mode is similar to that from the dipole. This is roughly $x = y \approx 17\mu m$, which is equivalent to a bunch size of about $\sqrt{2} \times 17\mu m \approx 30\mu m$.

Another limiting factor could be that the quadrupole signal itself could be too small to be detected above electronic noise. This analysis is the same as in Sec. IV. Assuming the measurable power ($P_{measurable}$) above electronic noise is 10^{-11}W, an rms-beam-size as small as 0.2μm can be measurable. Therefore, it is likely that the common mode effect limits the quadrupole measurement resolution. Considering imperfections in the hybrid networks, a power reduction of the monopole and dipole modes through the networks down by a factor of 10^{-5} (-50 dB) may be considered reasonable. This leads to a rms-beam-size resolution on the order of ten microns.

V. QUADRUPOLE CAVITY CALIBRATION

We have shown that the output voltage after the last hybrid *T* junction is from the TM_{220} cavity mode only and that this mode couples with the beam quadrupole moment. Therefore, the voltage is proportional to the beam quadrupole-moment.

$$V_q \propto \left(x_{L,b}^2 - y_{L,b}^2 + \sigma_{x_L}^2 - \sigma_{y_L}^2\right) \text{ in linac coordinates.} \tag{19}$$

In an ideal situation the proportionality constant of the equation can be evaluated. In practice, we need to determine the coefficient experimentally by a calibration, to include all the practical effects of a real physical system in the beamline.

The goal of this calibration is to determine the proportionality constant in the above equation. For a large number of beam pulses, the quad-output signal, when plotted as a function of x_L, looks like the plot shown in Fig. 10 (a). The plots in Fig. 10 are generated numerically by varying beam positions. It illustrates what a typical run might generate. Each pulse which may contain a train of bunches is represented as a dot in the figure. Each pulse is considered as a rigid pencil moving parallel to the axis. The spread in x_L is due to the beam x_L-positions, and the vertical spread is due to the variation in beam y_L-positions. The vertical spread, however, is bounded by a parabola. This "bounding parabola", consisting of pulses with $y_{L,b}$=0, provides the coefficient of proportionality. Furthermore, the quad-signal where the parabola crosses the x_L-axis gives the vale of $\sigma_{x_L}^2 - \sigma_{y_L}^2$. For a flat beam, the value is approximately the square of the rms-size in the larger dimension. Repeating the procedure using $y_{L,b}$ as the independent variable provides a crosscheck of the calibration factor. (See Fig. 10 (b).)

VI. FABRICATION CONSIDERATIONS

Phase errors may be introduced by asymmetries due to imperfections in fabrication, and thermal expansions. A 0.001" error in one of the iris locations and sizes can modify the resonant frequency by over 10 MHz. Therefore, it is crucial to fabricate the cavity with great accuracy.

Phase errors due to inaccuracies of the waveguide lengths are estimated not to be significant. Even when the two hybrid tee lengths differ by 120 microns, corresponding to an error of 1.6° for a signal of 11.424 GHz, only an insignificant amount of output power reduction is observed.

Tolerance with temperature variation is estimated before fabrication. For a resonant mode whose loaded quality factor, $Q_{Lq} \approx 750$, the 29.3% amplitude degradation level (-3dB) corresponds to $\delta f_q / f_q = 1/(2Q_{Lq}) \approx 6.7\times10^{-4}$. For the quad-cavity dimensions, this level of sensitivity allows a variation of a cavity dimension of $\delta a \approx 25$ μm (~0.001"), since $\delta a / a \approx -\delta f_q / f_q$. Using the thermal expansion coefficient of Cu of 16.5×10^{-6}/K, we find that this level of sensitivity corresponds to an allowable change in temperature of $\delta T \approx 40$°C.

Machining and brazing errors are also estimated before fabrication. With conventional CNC machining some corners must generally be radiused. The errors in the frequency from this can be estimated using the variational method. For the quadrupole mode, the 0.0625" rounded corners, parallel to the beampipe, modify the cavity resonant frequency by on the order of $10^{-5} f_q$. Similarly, 0.005" rounded corners, parallel to the cavity x- or y-axis, modify the cavity resonant frequency on the order of $10^{-5} f_q$. Therefore, adjustment of the dimensions due to these errors was deemed unnecessary.

After these considerations, our quad-cavity system was fabricated. (See Fig. 9.)

VII. EXPERIMENTAL RESULTS

A. RF tests and cavity tuning

The prototype cavity was designed and built with a push/pull mechanical impact tuning scheme.[13] This allows fine adjustment of the resonance frequency by a slight, azimuthally symmetric deformation of the cavity wall around the beam pipe. Machining tolerances could thus be looser than would otherwise be required.

Before final brazing of the hybrid network waveguides, rf tests were performed on the cavity with an HP8510 network analyzer, and the cavity resonance was fine tuned. With cavity fabrication specifications within 0.002" accuracy, the quadrupole resonance turned out to be 11.4096 GHz, 14.4 MHz below our goal. By slight impact compressions of the cavity, the resonant frequency was raised to the desired value of 11.424 GHz, as shown in Fig. 11.

B. Beam tests

The quad-cavity system was completely assembled as in Fig. 9, with the hybrid waveguide networks and an rf window for operation under vacuum. It was installed near the end of the beamline of the Next Linear Collider Test Accelerator (NLCTA) at the Stanford Linear Accelerator Center (SLAC). A waveguide-to-coax adaptor attached to the WR90 port and a low-loss heliax cable connected the cavity to the rf monitoring system outside the accelerator enclosure. There, the signal was down-mixed with an X-band reference signal through I-Q demodulators and digitized in a 1 gigasample/s digitizing scope to produce high-resolution phase and amplitude signals for individual beam pulses. Due to experimental limitations in these initial beam tests, we did not have the opportunity to fully demonstrate the monitor's capabilities and to characterize its resolution. Nevertheless, they did provide some useful results.

In time structure, the NLCTA beam is a bunch train with every 11.424 GHz rf bucket filled. Beam tests of the quad-cavity system were performed with beam pulse currents ranging from 40 mA to 350 mA and beam pulse lengths ranging from several nanoseconds to 105 ns. Fig. 12 shows two examples of signal pulses. Even short pulses produced adequate signal. From the time constant of the exponentially decaying signal pulses, the loaded quality factor Q_L of the monitor can be calculated. On average, we measured $Q_L = \omega\tau/2 \approx 1{,}100$, where ω is the angular frequency and τ the fitted e-folding time. This roughly agrees with an HFSS simulation including copper wall losses, which yielded $Q_L = 1{,}008$.

We were able to probe the cavity field pattern by steering the beam transversely in x_L and y_L by means of nearby corrector magnets. The signal amplitude from an x_L scan, with sign determined by the signal phase, is plotted in Fig. 13. The parabolic shape confirms that we are detecting the quadrupole mode excitation. Since we attempted to zero y_L for this scan, the fact that the plot passes through zero twice could be indicative of a non-zero beam quadrupole moment (See Eq. (3)).

Fig. 14 shows the variation of the signed cavity signal amplitude as the beam is moved over a 2-D grid of points in transverse coordinates x_L and y_L. The nice saddle shape clearly indicates again that the monitor is sensitive to the quadrupole mode. The range of the scan is approximately 5 mm along either direction, though we have had to leave the axes in arbitrary units, proportional to the corrector currents, because an independent measure of the exact beam position at the cavity could not be reliably obtained. The nearest BPM was about ten inches away, and the beam was sharply focused by an upstream quadrupole magnet. An attempt to infer the local position from the readings of two downstream BPM's using TRANSPORT matrices[14,15] from the NLCTA on-line model was unsuccessful, (it yielded a y_L-range slightly exceeding the beampipe aperture), presumably because the model needed updating.

In a subsequent run, only a shorter bunch train of a few nanoseconds was available, as the gun pulser was changed, and the beam was considerably larger near the cavity due to the removal of an upstream quadrupole magnet from the beam line. On the positive side, removal of the quadrupole magnet allowed us to better infer the beam position at the cavity by a linear trajectory between two BPM's. The larger beam led to some loss of beam current due to scraping as we moved the beam around. To correct for loss, the cavity signal was scaled by the inverse of the transmitted current. The end points of position scans show also some deviation from linearity in BPM-measured position with step number (in corrector magnet current). Since the correctors do not saturate in this range and there are no sextupoles in the beamline, the deviation in BPM readings was interpreted as an artifact of the current loss, as the clipping of one side of the current distribution moved the effective center of charge to the other side. A constant position change per step was thus imposed on the data based on a linear fit to the central points.

Fig. 15 shows the corrected signal as functions of corrected x_L- and y_L-position. Parabolic fits to this data determined the electrical center of the cavity to be approximately at x_L=0.501 mm and y_L=0.151 mm. Repeated measurement of x_L suggested a precision of about 40 µm. In general, a 2 D scan is required to determine the center, in case of slight cavity rotation. Such a scan over a grid in x_L and y_L was also attempted in this run, but was beset with problems, including excessive beam jitter and drift during the scan and a y_L-range not straddling the electrical center. Nevertheless, to illustrate the use of such data, we fit the quadrupole signal to a quadratic function,

$$V_q(\mathrm{x},\mathrm{y}) = V* + a\left(\left(\mathrm{x}_L - \langle \mathrm{x}_{L,b}\rangle\right)^2 - \left(y_L - \langle y_{L,b}\rangle\right)^2\right) \quad \text{where} \quad V* \equiv a\left(\sigma_{x_L}^2 - \sigma_{y_L}^2\right) \ , \qquad (20)$$

and found $\langle \mathrm{x}_{L,b}\rangle$ = 0.4773 mm, $\langle y_{L,b}\rangle$ = -0.5318 mm, $a =$ 0.4657 mm^{-2} and $V*$ = 0.7221.

The x_L-center is within 0.024 mm of the value from the linear scan (whereas the y_L-center value is unreliable due to one-sidedness of the data range). The beam quadrupole moment calculated from this fit is $\sigma_{x_L}^2 - \sigma_{y_L}^2 = V_* / a = \sim 1.551$ mm^2. The rms deviation of the data from the 2-D fit is 0.2728. Dividing this deviation by the quadratic coefficient a = 0.4657 and taking the square root, one obtains 0.765 mm as a measure of the 1-D resolution under these non-ideal conditions.

A major contributor to this large resolution is jitter in the beam position. We also measured the variation of the quadrupole signal for fixed corrector settings (and presumably fixed beam position) and found it had an rms variation of 6.3% of the average signal value of 0.2533 for 50 shots. Again, dividing by a and taking the square root, one obtains 0.18 mm as a measure of the beam jitter for this particular position. Taking into account only the rms fit deviation above, one would have $\sigma_{x_L}^2 - \sigma_{y_L}^2 =$ 1.551 ± 0.586 mm^2 or $\sqrt{\sigma_{x_L}^2 - \sigma_{y_L}^2} = 1.22 \pm 0.24$ mm. But the size of the beam jitter is already about 0.18 mm, and not independent of the rms fit deviation. Obviously, the data discussed here do not represent the beam size resolution ultimately achievable with this cavity.

While the above scanning experiment helps us understand its function, the intended use of this device is as a single shot quadrupole moment monitor. For such application, it must first be accurately calibrated with a small, well characterized beam or a wire test. In operation the position of the measured beam relative to the known electrical center of the cavity must be accurately determined by independent BPM's (and preferably zeroed), as well as its charge and bunch length.

VIII. DISCUSSION

As a figure of merit, we estimate from simulations that the quad-cavity system can measure a flat beam-size of much less than 100 microns and that it is robust enough against coupling of monopole and dipole modes to the quadrupole mode signal for small perturbations of the geometrical symmetry. At present, however, we do not have an experimental beam-test verification of the resolution. The beam tests discussed above provided, at most, qualitative results. Due to the limitations of beam diagnostics and beam conditions at the NLCTA, the possible beam size resolution obtainable was limited to only hundreds of microns. This measurement, therefore, does not represent the ultimate resolution achievable with this device. In the future, more calibration and beam tests may be performed if a suitable beam line should become available and there is interest in deploying this new beam diagnostic tool.

One of the main difficulties of the measurement was not being able to obtain the beam position at the quad-cavity location accurately. The quadrupole measurement would be much more accurate if the transverse beam position were measured at the same place. This observation led us to the development of an integrated multi-cell cavity beam monitor including position measurement [1].

The work reported in this paper was carried out as an application for the NLC beams. Recently, the NLC project has been subsumed into the ILC (International Linear Collider) project. However, the general concept and design presented in this paper may be directly applicable to beams in linear accelerators other than the NLC, such as those of the ILC.

IX. ACKNOWLEDGMENTS

Work supported by US Department of Energy under the grant DE-FG03-98ER82574 and the CRADA agreement, project 185, with Stanford Linear Accelerator Center. The project was in part supported by the grant DE-AC03-76SF00515.

The authors are indebted to D.H. Whittum for the original idea inspiring this work and set the ground work. We thank C. Pearson for assistance on the mechanical design and fabrication of the cavity, M. Ross, C. Adolphsen, K. Jobe and T. Smith for help with NLCTA installation and operations. Special thanks also go to W. Bruns for his kind help with the GdfidL code. We also thank W. Spence, J. Goldberg, D. Edgell, N. Barov, and S. Tantawi for their contribution to this project.

REFERENCES

[1] J.S. Kim, R.H. Miller, and C.D. Nantista, Rev. Sci. Instr. **76**, 073302 (2005).

[2] R.H. Miller, J.E. Clendenin, M.B. James, J.C. Sheppard, Proc. 12th Int. Conf. on High Energy Acc. (Fermilab, Batavia, 1983); SLAC-PUB-3186.

[3] A. Jansson, Phys. Rev. ST Accel. Beams 5:072803, (2002).

[4] D.H. Whittum, and Y. Kolomensky, Rev. Sci. Instr. **70**, 2300 (1999).

[5] J.S. Kim , C.D. Nantista, D.H. Whittum, R.H. Miller, S.G. Tantawi, and A.W. Weidemann, Proceedings of the 2001 Particle Accelerator Conference (PAC 2001), Chicago, IL, June 2001; SLAC-PUB-9420.

[6] C. D. Nantista, J. S. Kim, A.W. Weidemann, Proceedings of the 21st International Linac Conference (LINAC 2002), Gyeongju, Korea, Aug. 2002; SLAC-PUB-9501.

[7] D.H. Whittum, Proc. JAPAN-CERN-US Joint Accelerator School, Shonan, Japan, 1996; SLAC-PUB-7802.

[8] J.S. Kim,D. H. Whittum, and S. Hiramatsu, Proc. of HEACC Conf., Hamburg, Germany, (1992).

[9] D. H. Whittum, S. Hiramatsu, and J. S. Kim, IEEE Plasma Science 21, 170 (1993)

[10] HFSS version 9; Ansoft High Frequency Structure Simulation Code, Ansoft Corporation, Pittsburg, PA. <http://www.ansoft.com/>

[11] GdfidL, v1.1, Feb.18, 2000. W. Bruns; www.gfidl.de, Proceedings in Particle Acc. Conf., Vancouver, vol. 2 p 2651 (1997).

[12] John C. Slater, *Microwave Electronics*, D. Van Nostrand Co., Inc., New York, 1950, p. 81

[13] G.B. Bowden, private communication.

[14] K. Brown and R.V. Servranckx, SLAC-Pub-3381 July (1984).

[15] D.C. Carey, K.L. Brown, F. Rothacker, SLAC Report SLAC-R-95-462, (1995).

Table I. Zeroth-order cavity design, based on closed pillbox. Values are evaluated for the cavity dimensions in Eq.(13), with 1 nC, single-bunch off centered at *x*(mm) and *y*(mm). The *y*-dipole case is the same as that of x-dipole except x is replaced by y, and is not shown. The normal quadrupole mode, (TM_{310}-TM_{130}) / 2, is not shown.

	TM_{110} monopole	TM_{210} (or TM_{120}) *x*-dipole	TM_{220} quadrupole $x = y$	(TM_{310} +TM_{130}) / 2 monopole
Resonant frequency $(\omega_\lambda / 2\pi)$ in GHz	5.7120	9.0315	11.4240	12.772
Leading field harmonic	constant	x	xy	constant
Skin depth (μ)	0.88	0.7	0.62	0.59
Q_w (for OFE Copper)	7.3×10^3	9.1×10^3	1.0×10^4	1.1×10^4
k_λ (V/pC)	1.4	$0.034 x^2$	$0.00082\ x^2 y^2$	0.87
$[R/Q]$ (ohms)	159	$2.41\ x^2$	$0.0454\ x^2 y^2$	44
U_λ (μJ)	1.4	$0.034\ x^2$	$0.00082 x^2 y^2$	0.87
P_λ (Watt)	7	$0.21\ x^2$	$0.0057\ x^2 y^2$	6.5
P_λ (Watt) filtered around 11.424 *GHz*	3.3×10^{-8}	$9.1 \times 10^{-9} x^2$	$0.0057 x^2 y^2$	1.2×10^{-6}

Table II. Values of resonant frequency, wall Q, shunt impedance (R) and power output (P_{out}) for the 1 mm-beam offset for the NLC beams of 1nC per bunch operating at 714 MHz.

	***x*-Dipole** **(TM_{210} or TM_{120})** x_b=1mm, y_b=0	**Quadrupole** **(TM_{220})** $x_b = y_b = 1/\sqrt{2}\ mm$	**Monopole-like** **(TM_{310}+TM_{130})** x_b=y_b=0
f_λ	8.955 GHz	11.427 GHz	13.147 GHz
$Q_{w\lambda}$	8200	9800	11000
R [ohm]	19500	103	2.83×10^5
P_{out} [W] (assumed Q_e/Q_w=0.111)	895	4.69	1.30×10^4

FIGURE CAPTIONS

FIG. 1. Cavity cross-section and cavity coordinates (*x*, *y*, and *z)*. The *z*-axis is along the beampipe.

FIG. 2. Cavity orientation in the beamline and the linac coordinates (x_L, y_L, z). The *z*-axis is along the beampipe.

FIG. 3. Amplitudes of cavity voltage at resonance (top), and off resonance by $\delta f = f_0/(2Q_{L\lambda})$ and by $2\delta f$ (bottom).

FIG. 4. Asymptotic cavity voltage amplitudes.

FIG. 5. Beampipe size effect on the cavity resonant frequency. Shown are for the lowest modes: TM_{110} (solid circle), the two degenerate TM_{210} and TM_{120} modes (triangle), TM_{220} (diamond), and the next two higher modes. The two highest frequency modes, degenerate in a closed pillbox, decouple with a beampipe: TM_{310}+TM_{130} (open circle) and TM_{310}-TM_{130} (cross).

FIG. 6. Full rf structure geometry with 3-T combining network to reject non-quadrupole modes (left figure). E_z-Contour plot of the 11.424 GHz TM_{220} mode (right figure)

FIG. 7. Output voltages of 1 nC-bunch off-axis at $x = y = 0.05$ cm, modeled by GdfidL: V1 of one bunch (top); V1-V2 of one bunch (second plot); V1-V2 for 80 ns pulse (third plot); and V1+V2 for 80 ns pulse (bottom).

FIG. 8. Fourier spectrum of the output voltages of 1 nC-bunch off-axis at x = y = 0.05 cm, modeled by GdfidL: Fourier spectrum of one bunch V1 (top); Fourier spectrum of one bunch V1+V2 (second plot); and Fourier spectrum of one bunch V1-V2 (third plot). Then multi-bunch results are shown for bunches operating at 11.424 GHz: Fourier spectrum of V1+V2 over 900 bunches (fourth plot); and Fourier spectrum of V1-V2 over 900 bunches (bottom).

FIG. 9. (top figure) A fully assembled emittance measurement quad-cavity system including an rf window (shown) and co-ax adaptor (not shown) and (bottom figure) the cavity with coupled T arms before brazing on top cover.

FIG. 10. Quad-cavity signals of many beam pulses projected on the x-axis for calibration (left figure) and quad-cavity signals of many beam pulses projected on the y-axis for calibration (right figure).

FIG. 11. The S_{12} signals between the waveguide port and a probe in the beampipe before (right peak) and after (left peak) fine tuning the cavity to 11.424 GHz.

FIG. 12. Cavity signal responses (arbitrary units) to a) a 105 ns beam pulse and b) a 15 ns beam pulse.

FIG. 13. Response as a function of beam position.

FIG. 14. 2-D surface and contour plots of the cavity response as a function of x_L and y_L corrector step (arbitrary units, linear with position).

FIG. 15. Signal (arbitrary units) versus corrected position and fit for a) an x_L-scan and b) a y_L-scan.

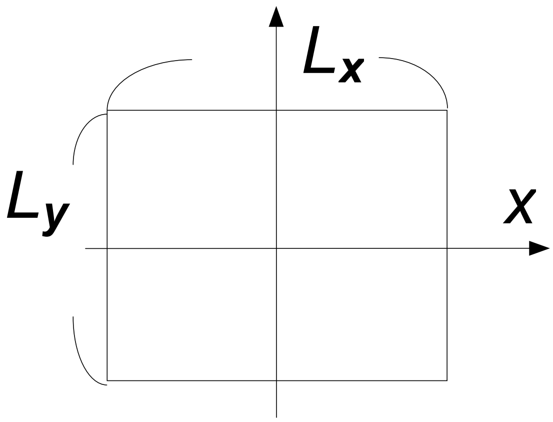

L_x
L_y
X

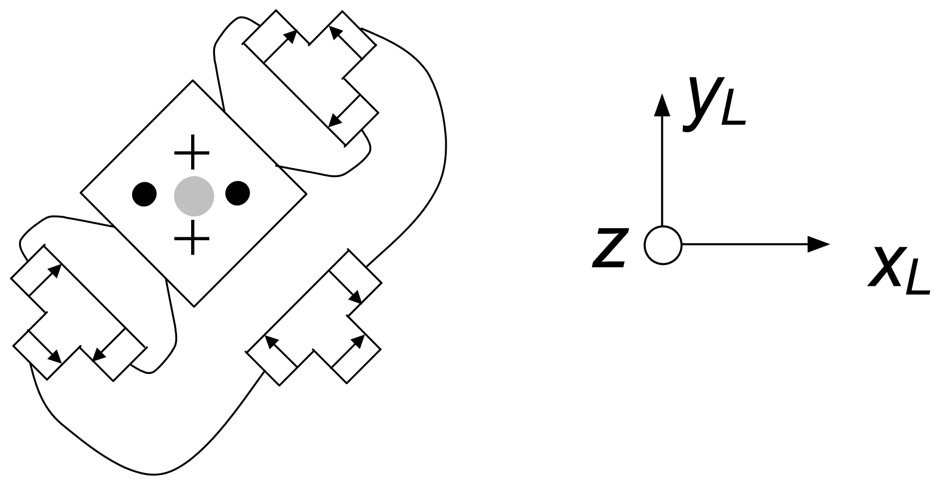

y_L
z
x_L

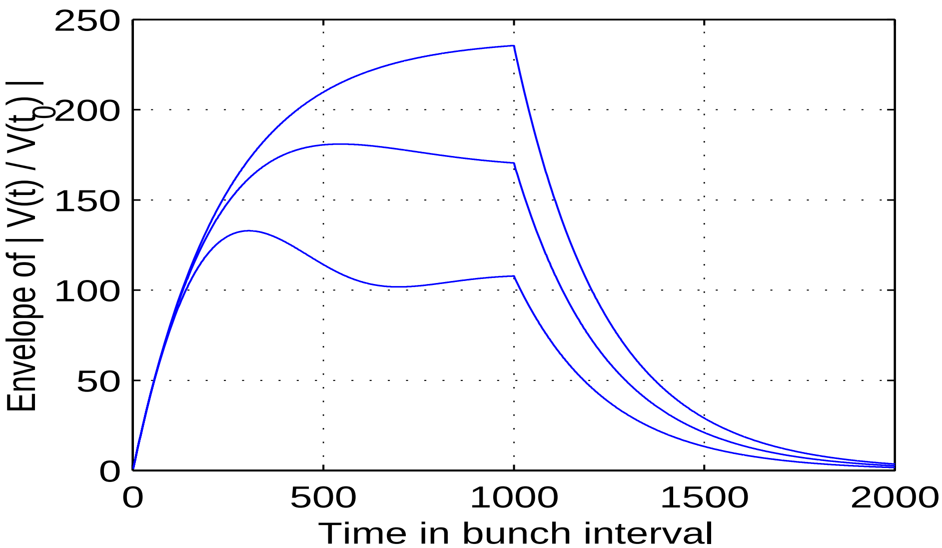

250
200
150
100
50
0
0
500
1000
1500
2000
Time in bunch interval
Envelope of | V(t) / V(t0) |

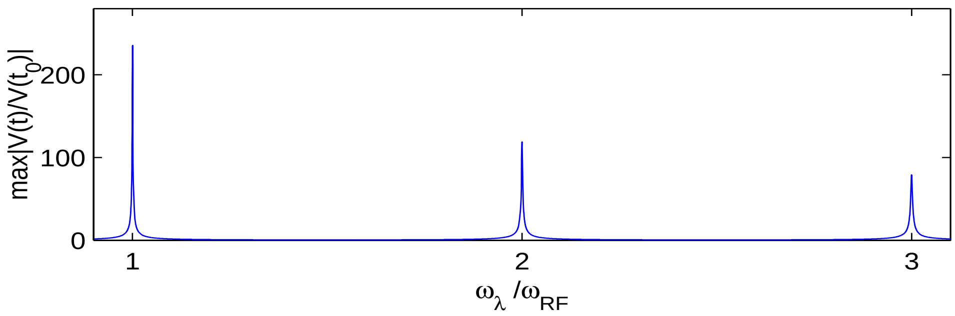

max|V(t)/V(t_0)|
200
100
0
1
2
3
ω_λ /ω_RF

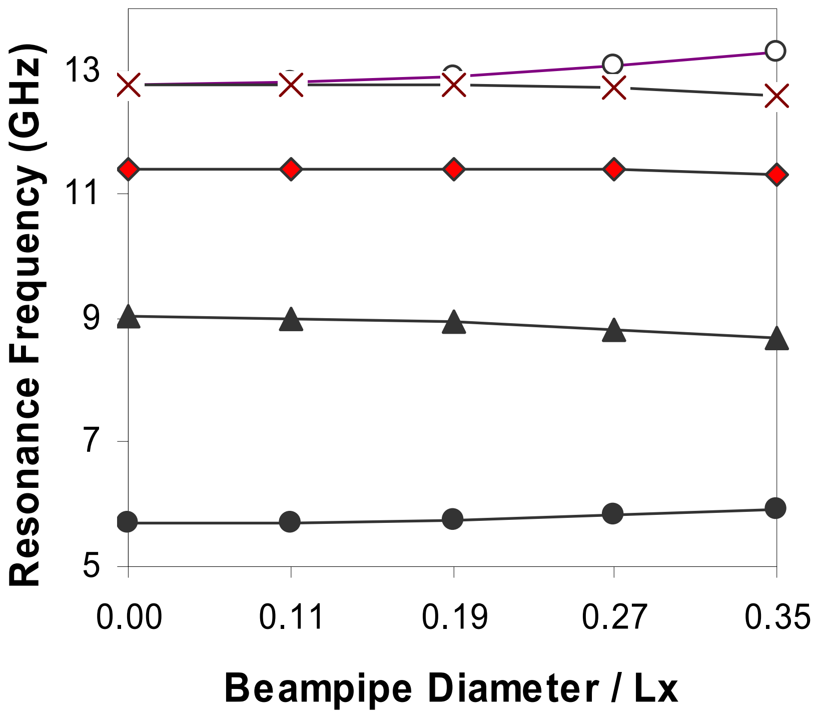

Resonance Frequency (GHz)
5
7
9
11
13
0.00
0.11
0.19
0.27
0.35
Beampipe Diameter / Lx

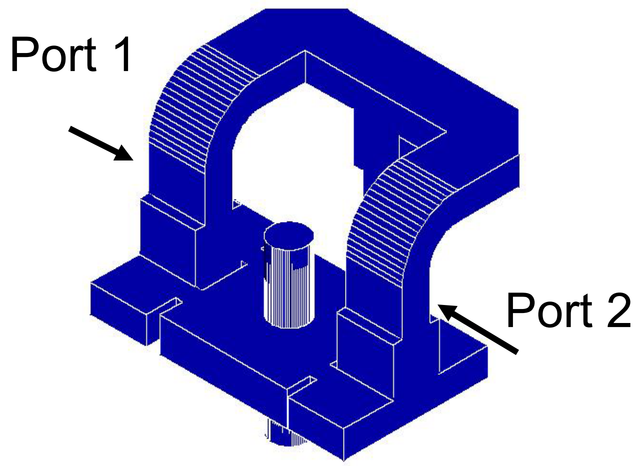
Port 1
Port 2

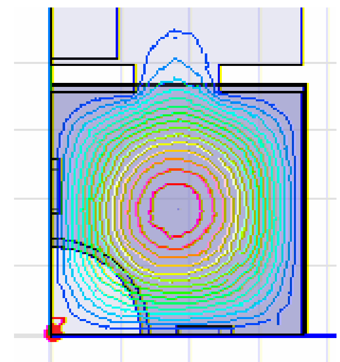

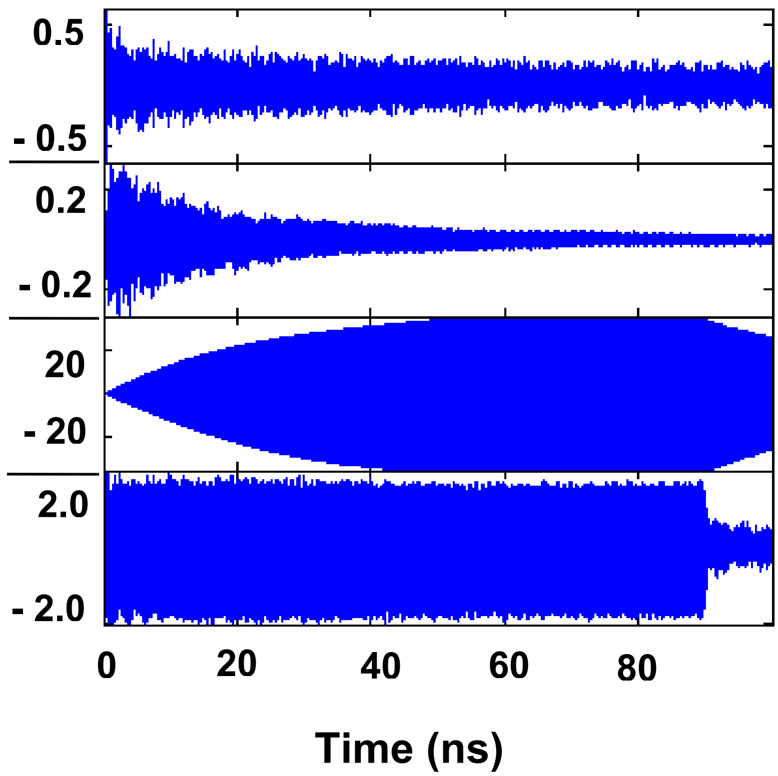
0.5
- 0.5
0.2
- 0.2
20
- 20
2.0
- 2.0
0
20
40
60
80
Time (ns)

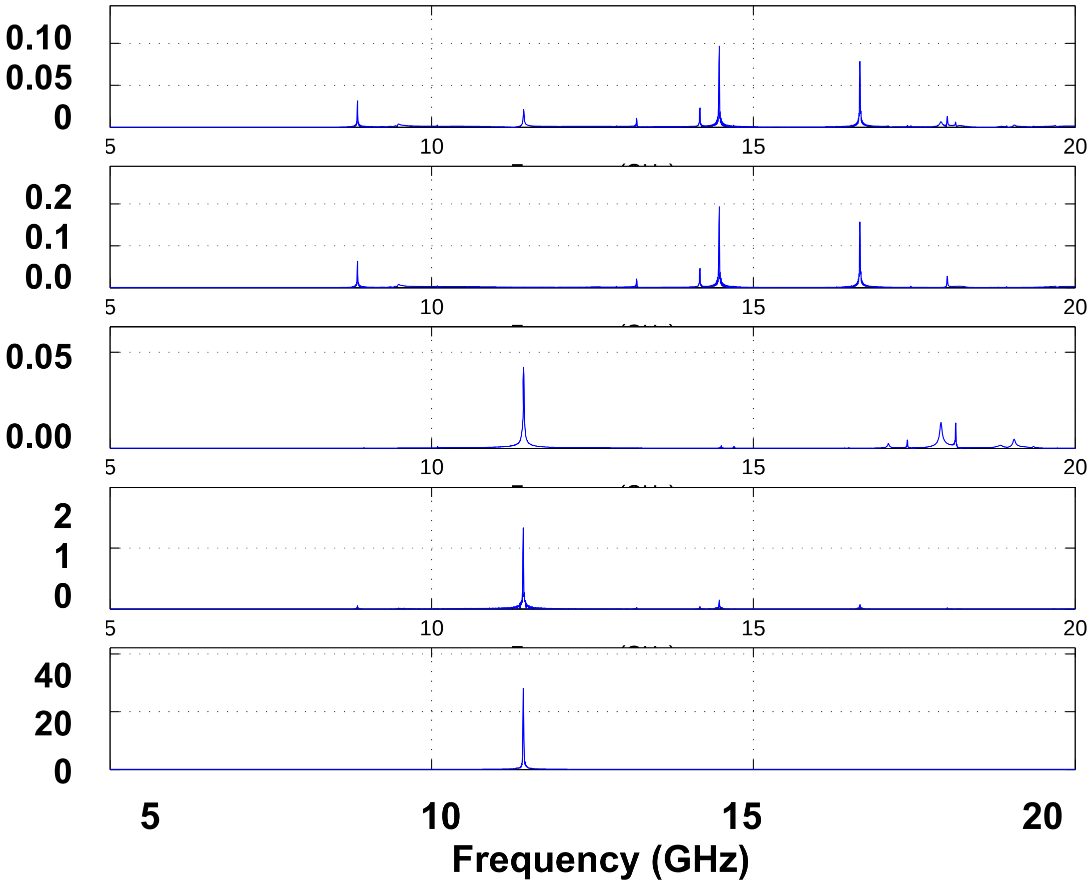
0.10
0.05
0
0.2
0.1
0.0
0.05
0.00
2
1
0
40
20
0
5
10
15
20
Frequency (GHz)

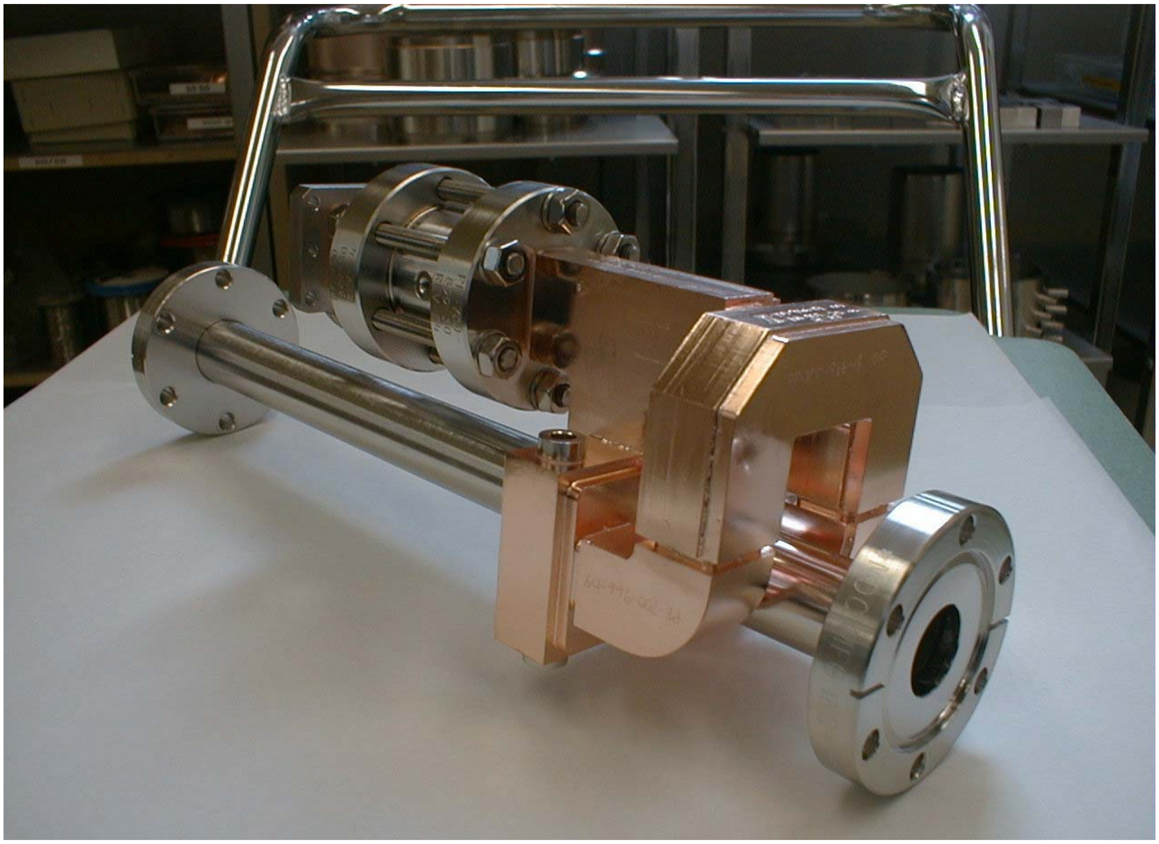

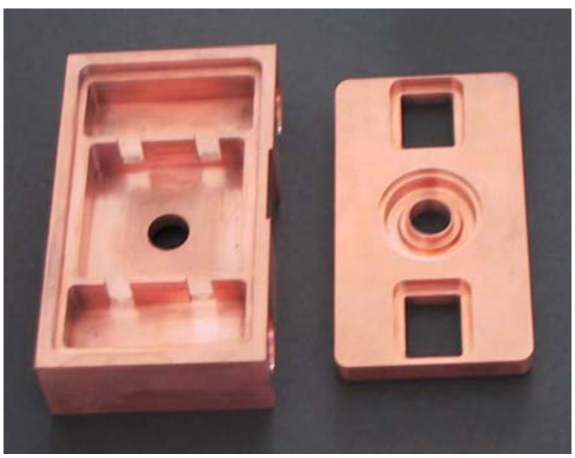

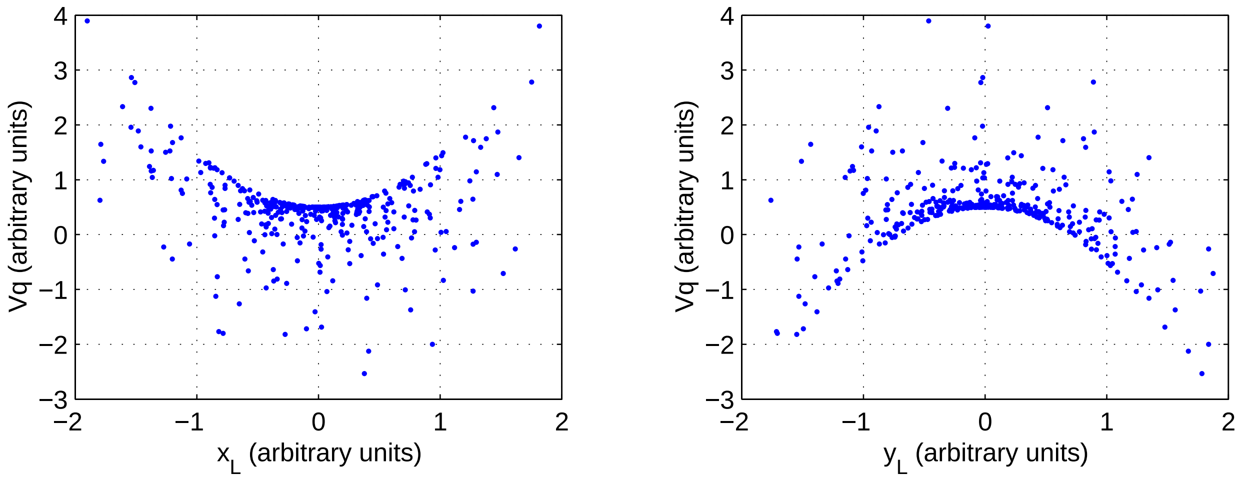

Vq (arbitrary units)
x_L (arbitrary units)
Vq (arbitrary units)
y_L (arbitrary units)

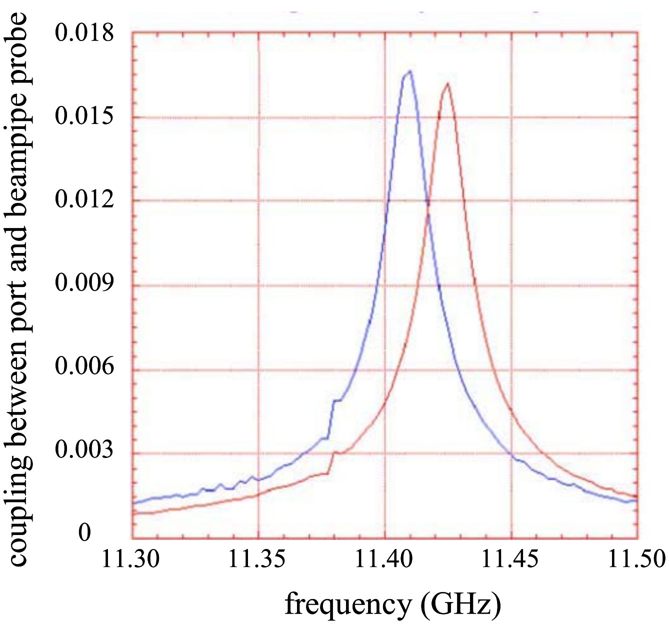
coupling between port and beampipe probe
0.018
0.015
0.012
0.009
0.006
0.003
0
11.30
11.35
11.40
11.45
11.50
frequency (GHz)

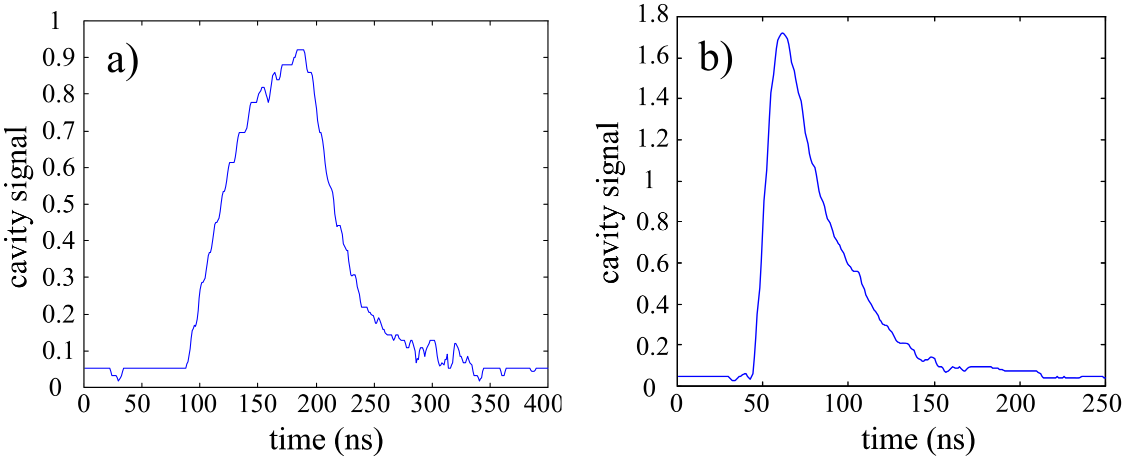

a)
cavity signal
time (ns)
0
0.1
0.2
0.3
0.4
0.5
0.6
0.7
0.8
0.9
1
0
50
100
150
200
250
300
350
400
b)
cavity signal
time (ns)
0
0.2
0.4
0.6
0.8
1
1.2
1.4
1.6
1.8
0
50
100
150
200
250

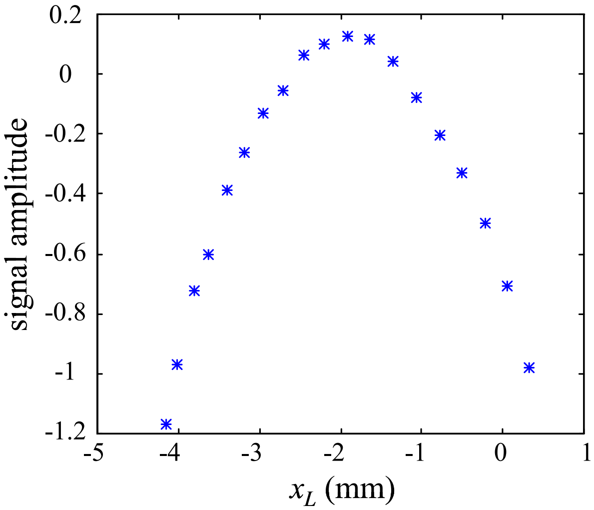
signal amplitude
0.2
0
-0.2
-0.4
-0.6
-0.8
-1
-1.2
-5
-4
-3
-2
-1
0
1
x_L (mm)

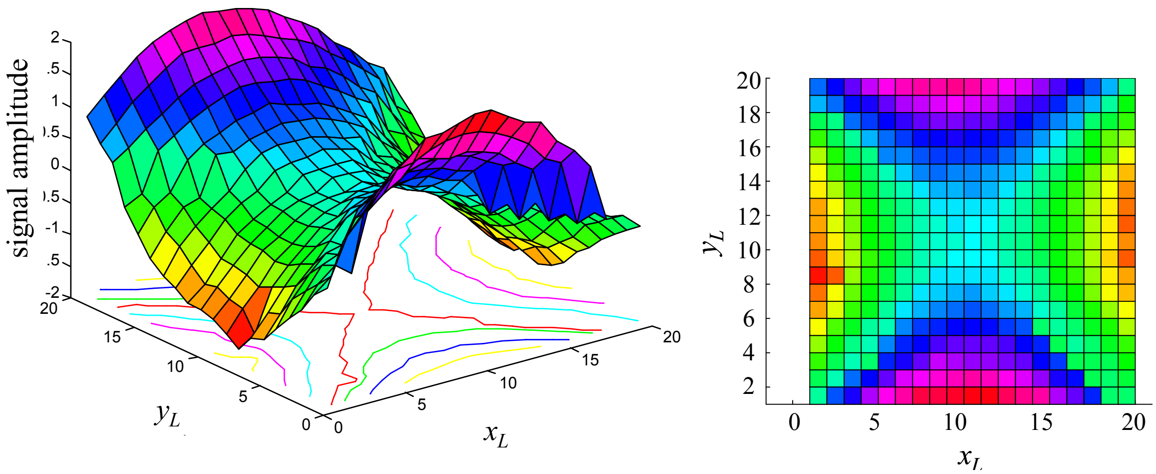

signal amplitude
2
.5
1
.5
0
.5
-1
.5
-2
20
15
10
5
0
y_L
0
5
10
15
20
x_L
20
18
16
14
12
10
8
6
4
2
y_L
0
5
10
15
20
x_L

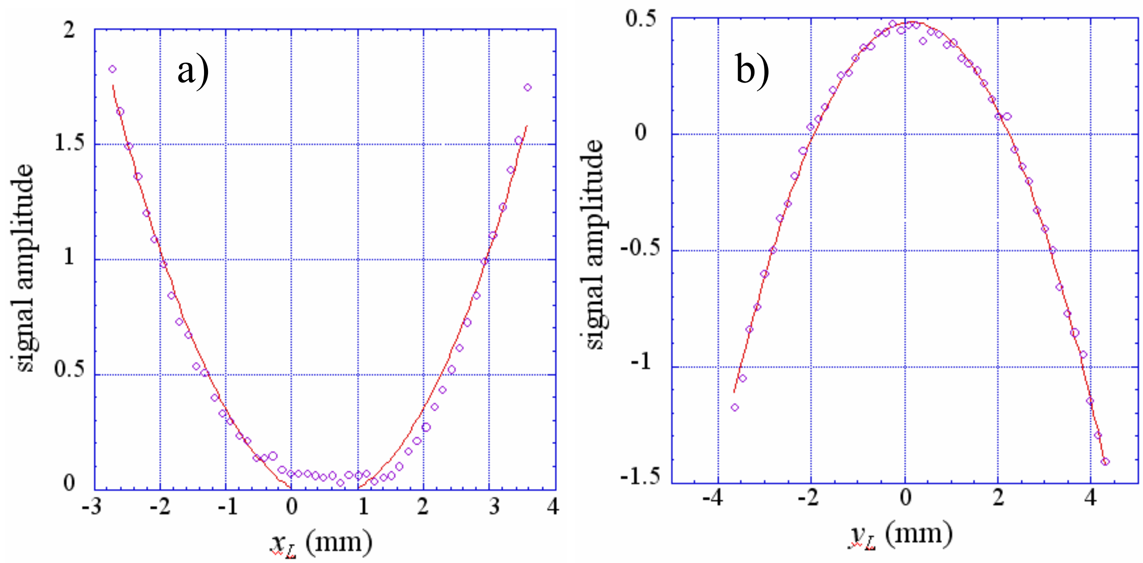

a)
signal amplitude
x_L (mm)
2
1.5
1
0.5
0
-3
-2
-1
0
1
2
3
4
b)
signal amplitude
y_L (mm)
0.5
0
-0.5
-1
-1.5
-4
-2
0
2
4